Electrical and Microstructural Aging of Porous Lanthanum Strontium Manganite/Yttria-Doped Cubic Zirconia Electrodes

M. C. Brant,[†,‡] T. Matencio,[†] L. Dessemond,[‡] and R. Z. Domingues*[,†]

Departamento de Química, Instituto de Ciencias Exatas, Universidade Federal de Minas Gerais, CP 702—CEP 31270-901, Belo Horizonte (Minas Gerais), Brazil, and Laboratoire d'Electrochimie et de Physico-Chimie des Materiaux et des Interfaces, Ecole Nationale Superieure d'Electrochimie et d'Electrometalurgie de Grenoble, No. 1130 Rue de la piscine, 38402 Saint Martin D'Heres Cedex, France

Received August 15, 2000. Revised Manuscript Received July 9, 2001

The formation of insulating phases at the interface between cathode and electrolyte materials during solid oxide fuel cell (SOFC) operation leads to deleterious effects on SOFC properties. We report in situ impedance spectroscopy measurements of the degradation process of porous $La_{0.65}Sr_{0.35}MnO_3/Zr_{0.84}Y_{0.16}O_{1.92}$ electrodes submitted to annealing temperatures above normal SOFC operating temperature, which is around 1173 K, simulating long-term SOFC operation. To measure the remaining effects after high-temperature annealing, impedance diagrams were plotted during the entire heating process up to the annealing temperatures, and during the complete cooling process. These diagrams were also plotted during the aging periods to follow the overall degradation. It was possible to detect and quantify electrical and electrochemical degradations, which are related to the formation of insulating phases at the electrode/electrolyte interface. Samples were annealed for about 200 h in air at temperatures between 1373 and 1673 K. Scanning electron microscopy and energy-dispersive X-ray spectrometry were also used to detect microstructural changes at the electrode.

1. Introduction

The common cathode and electrolyte materials for the conventional solid oxide fuel cell (SOFC) are strontium-doped lanthanum manganite (LSM) and yttria-stabilized zirconia (YSZ), respectively. LSM is chosen due to its advantageous properties such as high conductivity,[1−4] chemical stability,[5] thermal expansion coefficient close to that of zirconia,[2,4] and low electrode overpotential.[6] It is supposed that the LSM/YSZ electrode reaction occurs in a narrow zone along the three-phase boundary (TPB), where the cathode material, the solid electrolyte, and the gas are in contact.[7−12] Better electrochemical performances are expected for electrodes with a higher TPB length per area. The operation temperature of conventional SOFCs is around 1273 K, and their components must be sintered at higher temperatures to achieve a good adhesion between electrode and electrolyte materials. These temperature conditions[13,14] can result in the formation of insulating phases at the electrode/electrolyte interface,[15−19] which promotes deleterious effects on SOFC properties.[5,20−23] The chemical

* To whom correspondence should be addressed. E-mail: rozanazd@dedalus.lcc.ufmg.br.

† Universidade Federal de Minas Gerais.

‡ ENSEEG.

(1) Kertes, M.; Riess, I.; Tannhauser, D. S.; Langpape, R.; Rohr, F. J. *Solid State Chem.* **1982**, *42*, 125.

(2) Hammouche, A.; Schouler, E. J. L.; Henault, M. *Solid State Ionics* **1988**, *28−30*, 1205.

(3) Hammouche, A.; Siebert, E.; Hammou, A. *Mater. Res. Bull.* **1989**, *24*, 367.

(4) Li, Z.; Behruzi, M.; Fuerst, L.; Stöver, D. In *Proceedings of the Third International Symposium on Solid Oxide Fuel Cells*; Singhal, S. C., Iwahara, H., Eds.; The Electrochemical Society: Pennington, NJ, 1993; Vol. 4, p 171.

(5) Yamamoto, O.; Takeda, Y.; Kanno, R.; Noda, M. *Solid State Ionics* **1987**, *22*, 241.

(6) Takeda, Y.; Kanno, R.; Noda, M.; Yamamoto, O. *J. Electrochem. Soc.* **1987**, *134*, 2659.

(7) Hammouche, A.; Siebert, E.; Kleitz, M.; Hammou, A. In *Proceedings of the First International Symposium on Solid Oxide Fuel Cells*; Singhal, S. C., Ed.; The Electrochemical Society: Pennington, NJ, 1989; Vol. 11, p 265.

(8) Mizusaki, J.; Tagawa, H.; Tsuneyoshi, K.; Sawata, A. *J. Electrochem. Soc.* **1991**, *138*, 1867.

(9) Haart, L. G. J.; Kuipers, R. A.; Vries, K. J.; Burggraaf, A. J. *J. Electrochem. Soc.* **1991**, *138*, 1970.

(10) Carter, S.; Selcuk, A.; Chater, R. J.; Kajda, J.; Kilner, J. A.; Steele, B. C. H. *Solid State Ionics* **1992**, *53−56*, 597.

(11) Kleitz, M.; Kloidt, T.; Dessemond, L. In *Proceedings of the 14th Riso International Symposium on Material Science*; Poulsen, F. W., Bentzen, J. J., Jacobseen, T., Skou, E., Ostergaard, M. J. L., Eds.; Riso National Laboratory: Roskilde, Denmark, 1993; p 89.

(12) Minh, N. Q. *J. Am. Ceram. Soc.* **1993**, *76*, 563.

(13) Yamamoto, O.; Takeda, Y.; Kanno, R.; Kojima, T. In *Proceedings of the First International Symposium on Solid Oxide Fuel Cells*; Singhal, S. C., Ed.; The Electrochemical Society: Pennington, NJ, 1989; Vol. 11, p 241.

(14) Roosmalen, J. A. M.; Cordfunke, E. H. P. *Solid State Ionics* **1992**, *52*, 303.

(15) Lau, S. K.; Singhal, S. C. *Proc. Corros.* **1985**, *85*, 79.

(16) Clausen, C.; Bagger, C.; Bilde-Sorensen, J. B.; Horsewell, A. In *Proceedings of the 14th Riso International Symposium on Material Science*; Poulsen, F. W., Bentzen, J. J., Jacobseen, T., Skou, E., Ostergaard, M. J. L., Eds.; Riso National Laboratory: Roskilde, Denmark, 1993; p 237.

(17) Tricker, D. M.; Stobbs, W. M. In *Proceedings of the 14th Riso International Symposium on Material Science*; Poulsen, F. W., Bentzen, J. J., Jacobseen, T., Skou, E., Ostergaard, M. J. L., Eds.; Riso National Laboratory: Roskilde, Denmark, 1993; p 453.

(18) Clausen, C.; Bagger, C.; Bilde-Sorensen, J. B.; Horsewell, A. *Solid State Ionics* **1994**, *70−71*, 59.

(19) Jiang, S. P.; Love, J. G.; Zhang, J. P.; Hoang, M.; Ramprakash, Y.; Hughes, A. E.; Badwall, S. P. S. *Solid State Ionics* **1999**, *121*, 1.

10.1021/cm000656r CCC: $20.00
Published on Web 10/13/2001

nature of the reaction product between LSM and YSZ depends on the strontium content of the electrode material.[24,25] Up to 30 mol % Sr, lanthanum zirconate ($La_2Zr_2O_7$) is mainly formed.[13−15,21,24−26] At higher concentrations, the formation of strontium zirconate ($SrZrO_3$) increases.[5,14,27] A-site deficiency in LSM has been shown to prevent the formation of these zirconate phases to a certain extent.[13] Besides chemical composition and temperature, the microstructure is another major factor that affects the cathode electrochemical properties.[28] The porosity must be large enough to ensure a fast oxygen supply to the reaction sites.[5,29,30] However, large porosity and large pore size lead to a shorter TPB length, and consequently to a detrimental effect on the cathode conductivity.[9] Another feature to consider in SOFC degradation is that a decrease in the effective electrode area will cause inhomogeneous current density distribution within the electrolyte, which may result in higher ohmic losses.[31]

Porous LSM electrodes containing 35 mol % Sr were used in this study. Two factors guided this choice. First, it has been reported[14] that, at this composition, both lanthanum and strontium zirconates may form and develop above about 1350 K. The second factor is that below this temperature no chemical reaction is expected to occur.[14] From this information, it is possible to preview the temperature at which electrical property modifications associated with interface chemical reactivity are expected to start.

The purpose of our work was to investigate how the growth of zirconate phases influences the electrical and electrochemical resistances of the LSM/YSZ interfaces. The samples were submitted to high annealing temperatures to accelerate solid-state reactions at the LSM/YSZ interface, simulating longer operation times. The resulting electrical and electrochemical degradation was followed by impedance spectroscopy. This technique allows the electrolyte electrical contributions and those of the electrode electrochemical behavior, separately, to be detected and quantified.[32]

2. Experimental Section

2.1. Sample Preparation. Electrolyte pellets were prepared from a $Zr_{0.84}Y_{0.16}O_{1.92}$ (YSZ) commercial powder provided by Tosoh Corp. After the powder was isostatically pressed and sintered at 1773 K for 2 h in air, the final density was around 98% of the theoretical value. Cylindrical pellets 0.099 ± 0.001 cm thick and 1.82 ± 0.01 cm in diameter were machined with diamond tools.

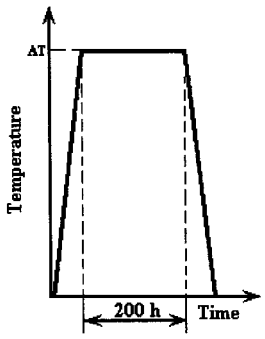

Figure 1. Simplified thermal cycle of $La_{0.65}Sr_{0.35}MnO_3/Zr_{0.84}Y_{0.16}O_{1.92}/La_{0.65}Sr_{0.35}MnO_3$ cells. AT is the annealing temperature (1373, 1473, 1573, or 1673 K).

The slurries used to produce porous electrodes were prepared from a mixture of 20 wt % $La_{0.65}Sr_{0.35}MnO_3$ solid solution commercial powder (SSC Inc.), 32 wt % linen oil, and 48 wt % turpentine extract. This mixture was homogenized in a blender containing zirconia balls and painted onto both sides of the YSZ surfaces. The assemblies were then fired at 1373 K for 2 h in air.

Low-angle X-ray diffraction patterns (Fe wavelength) of the as-fired LSM/YSZ interface confirmed the absence of chemical reaction during the firing procedure.

2.2. Microstructural Analyses. Microstructural and compositional analyses were performed on the LSM surface, and on the LSM/YSZ cross-section before and after the annealing periods. An electron microprobe analyzer apparatus (JEOL JXA-8900) was used to record the scanning electron microscopy (SEM) and energy-dispersive X-ray spectrometry (EDS) analyses.

2.3. Electrical Measurements. Impedance spectroscopy (IS) measurements were carried out on symmetrical cells in air. A platinum grid was used as a current collector. Impedance diagrams were recorded under zero dc conditions. Measurements in the low-frequency range, $10^{-3}-10^4$ Hz, were obtained by an Autolab potentiostat/impedance frequency analyzer (Eco-Chemie). For higher frequencies, $(5-1.3) \times 10^7$ Hz, a Hewlett-Packard impedancemeter (HP 4192 A LF) was used. The amplitude of the ac signal was 30 mV. Identical impedance values were obtained for the same cells within the common frequency interval of both apparatuses. The amplitude of the ac signal was varied to verify the linear behavior of electrical properties of the LSM/YSZ interface and also to ensure that the relaxations observed were related to the charge transport through and in the vicinity of the interfaces. Hereafter, the numbers shown in the impedance diagrams indicate the logarithm of the measuring frequency.

Impedance diagrams were plotted every 50 K between 523 and 1223 K during both the heating and cooling cycles and at the annealing temperature to follow the overall degradation, and to measure the conductivity changes after annealing. Figure 1 summarizes the thermal cycle of the samples tested.

The interpretation of the IS spectra obtained in this study is based on the equivalent electrical circuit model.[33] The polycrystalline electrolyte sample diagram usually comprises three arcs (Figure 2): the first, located at higher frequencies, has been ascribed to the electrolyte grains (electrolyte specific impedance), the second, located in the intermediate frequency range, is due to the microstructure blockers (blocking impedance), and third is related to the electrode reaction (electrochemical overpotential impedance).

Sometimes the second arc can be deconvoluted into several semicircles. It is due to the presence of additional microstruc-

(20) Poulsen, F. W.; Van der Puil, N. *Solid State Ionics* **1992**, *53−56*, 89.
(21) Kenjo, T.; Nishiya, M. *Solid State Ionics* **1992**, *57*, 295.
(22) Chen, C. C.; Nasrallah, M. M.; Anderson, H. U. In *Proceedings of the Third International Symposium on Solid Oxide Fuel Cells*; Singhal, S. C., Iwahara, H., Eds.; The Electrochemical Society: Pennington, NJ, 1993; Vol. 4, p 252.
(23) Lee, H. Y.; Oh, S. M. *Solid State Ionics* **1996**, *133−140*, 90.
(24) Yokokawa, H.; Sakai, N.; Kawada, T.; Dokiya, M. *Solid State Ionics* **1990**, *40−41*, 398.
(25) Yokokawa, H.; Sakai, N.; Kawada, T.; Dokiya, M. *J. Electrochem. Soc.* **1991**, *139*, 2719.
(26) Mitterdorfer, A.; Gauckler, L. J. *Solid State Ionics* **1998**, *111*, 185.
(27) Setoguchi, T.; Inoue, T.; Takebe, H.; Eguchi, K.; Mornaga, K.; Arai, H. *Solid State Ionics* **1990**, *37*, 217.
(28) Ostergaard, M. J. L.; Clausen, C.; Bagger, C.; Mongensen, M. *Electrochim. Acta* **1995**, *40*, 1971.
(29) Suzuki, M.; Sasaki, H.; Kajimura, A.; Sugijura, N.; Ippommatsu, M. *J. Electrochem. Soc.* **1994**, *141*, 1928.
(30) Sasaki, H.; Suzuki, M.; Sogi, T.; Kajimura, A.; Yagasaki, E. In *Proceedings of the Fourth International Symposium on Solid Oxide Fuel Cells*; Dokiya, M., Yamamoto, O., Tagawa, H., Singhal, S. C., Eds.; The Electrochemical Society: Pennington, NJ, 1995; Vol. 1, p 187.
(31) Schouler, E. J. L. *Solid State Ionics* **1983**, *9−10*, 945.
(32) Brant, M. C.; Dessemond, L. *Solid State Ionics* **2000**, *138*, 1.
(33) Boukamp, B. A. *Solid State Ionics* **1986**, *20*, 31.

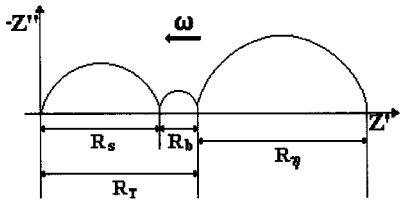

Figure 2. Usual complex impedance diagram for systems involving polycrystalline electrolytes. R_s is the specific resistance of the electrolyte grains, R_T is the interfacial resistance, and R_η is the electrochemical overpotential resistance.

ture blockers such as second-phase inclusions, pores, and cracks besides the grain boundaries. These blockers immobilize a fraction of the matrix charge carriers because of strong distortions of surrounding current lines.[34] For the sake of simplicity, in this work the overall impedance of both YSZ grains and blocking contributions will be referred to as interface impedance. Figure 2 shows the interface resistance (R_T) calculated from the addition of the electrolyte specific resistance (R_s) and the blocking resistance (R_b).

The electrode characteristics can be composed of two or three more or less overlapping semicircles, but nowadays, there is no generally accepted method to deal with the interpretation of the electrochemical part of the impedance diagram. The determination of the elementary steps of the electrode reaction is beyond the scope of this paper. All the electrode characteristics recorded on the investigated specimens are typical of porous LSM-based cathodes. The electrochemical overpotential resistance (R_η) was determined from the difference between the low-frequency intercept of the electrode characteristic with the real axis in the complex impedance plane and the high-frequency interface resistance (Figure 2). Both R_T and R_η were considered in this study.

3. Results and Discussion

Figure 3 shows SEM micrographs of an as-fired LSM/YSZ sample. The bright field in Figure 3a shows a porous LSM film deposed on a dense YSZ pellet. The film is relatively homogeneous and presents a layer thickness of about 4 μm. A good adhesion was achieved between the electrode material and the electrolyte. After firing, the mean grain size of the LSM particles was around 0.3 μm (Figure 3b).

Figure 4a shows a typical interface impedance diagram obtained at 673 K for samples before annealing, similar to those generally recorded on Pt/polycrystalline yttria-stabilized zirconia/Pt samples.[35] The diagram is composed of the high-frequency semicircle of the YSZ grains and the low-frequency blocking effect due to the regular grain boundaries. The shapes of the impedance diagrams recorded before any annealing are very similar for all the samples investigated, regardless of the temperature and frequency range analyzed. This fact confirms the homogeneity of the electrolyte and the reproducibility of the surface electrode coverage for the as-fired LSM/YSZ samples.

The variation of the interface resistance R_T was evaluated during each annealing. The additional interface resistance, ΔR_T, was determined by the mathematical difference between the interface resistance measured at a given time t and the initial one (at $t = 0$).[32] A positive ΔR_T value indicates the presence of an additional resistance effect at a given measurement time. The deleterious increase in ΔR_T during the annealing time is called the aging effect of the interface resistance. The term "aging effect" implies that the degradation effect increases with the annealing time. The relative increase in the additional interface resistance, defined as the ratio $\Delta R_T/R_T$ (both measured at time t during the course of high-temperature annealing), was also used in this study to scale the degradation rates recorded. It represents the additional fraction of the electrical charge that is blocked due to the aging degradation effect.

Figure 5a shows the variations of ΔR_T during annealing as a function of annealing time at all the annealing temperatures. Figure 5b gives the time evolution of $\Delta R_T/R_T$. At 1373 K, the characteristics of the LSM/YSZ interface are not significantly changed. However, when the measuring temperature was decreased after annealing to 673 K (Figure 4b), the interfacial resistance R_T was about 16% larger, if compared to that before annealing (Figure 4a). This residual effect at 673 K can be observed for both the high-frequency part of the electrolyte and the blocking impedance (Figure 4b). Annealing at 1473 K produced a positive effect at the first 100 h (Figure 5a). Up to this time, both ΔR_T and $\Delta R_T/R_T$ values decreased, which means an improvement in the electrical conduction (Figure 5). After 100 h the interface resistance increased, following a square root law with time (Figure 5a). The period before the beginning of the interface electrical degradation is called the induction period, because it can be associated with the induction period of the chemical reaction between lanthanum manganites and YSZ.[13,26,36] This induction period can be explained by a favorable initial diffusion of Mn ions from the manganite into YSZ, up to a point at which the lanthanum manganite phase near the YSZ becomes much deficient in Mn, and enriched in La (and/or Sr). At this point the diffusion of Mn into YSZ stops, and the chemical reaction takes place.[36] The introduction of Mn into the YSZ grain boundary can be responsible for the initial decrease in the interface resistance observed at the early stage of Figure 5 by diminishing the interface resistance.[37,38] The square root dependence of R_T recorded above 100 h suggests a diffusion-controlled mechanism for the interface electric degradation. This diffusion-controlled mechanism can be related to the formation of zirconate phases at the LSM/YSZ interface. The supply of cations by diffusion to the chemical reaction zone may be the determining process for the formation of the zirconate phases, since cationic conductivity must be lower than anionic conductivity in both LSM and YSZ.[14,26] The diffusion can be described by Fick's second law, which can be simplified to show a square root dependence of the amount of the reaction product on the reaction time.[14] From an electric point of view, foreign zirconate phases at the LSM/YSZ interface can be considered as additional microstructure blockers.[34,32] Therefore, an increase in R_b and, consequently, in R_T could be expected. Thus, even small quantities of zirconate phases can be detected by IS. For

(34) Dessemond, L.; Muccillo, R.; Hénault, M.; Kleitz, M. *Appl. Phys.* **1993**, *A57*, 57.
(35) Kleitz, M.; Bernard, H.; Fernandez, E.; Schouler, E. In *Advances in Ceramics*; Hever, A. H., Hoods, L. W., Eds.; The American Ceramic Society: Columbus, 1981; Vol. 3, p 310.
(36) Taimatsu, H.; Wada, K.; Kaneko, H. *J. Am. Ceram. Soc.* **1992**, *75*, 401.
(37) Kim, J. H.; Choi, G. M. *Solid State Ionics* **2000**, *130*, 157.
(38) Appel, C. C.; Bonanos, N. *J. Eur. Ceram. Soc.* **1999**, *19*, 851.

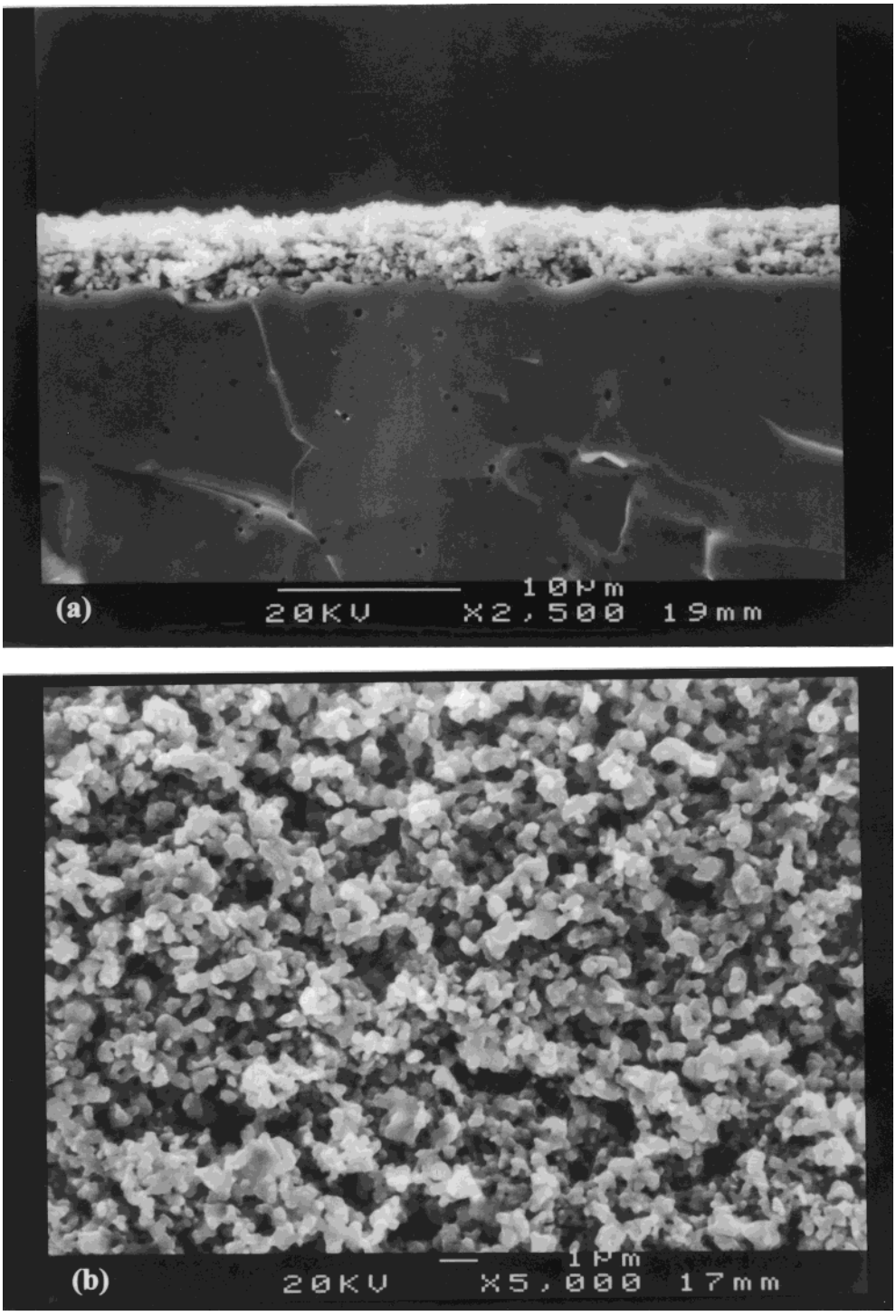

Figure 3. Scanning electron micrographs of a $La_{0.65}Sr_{0.35}MnO_3/Zr_{0.84}Y_{0.16}O_{1.92}$ sample fired at 1373 K (2 h): (a) cross-section and (b) LSM surface.

the sample aged at 1573 K, the induction period was reduced to 16 h and the degradation rate was higher (Figure 5a). This thermally activated phenomenon has already been observed by using pin-shaped LSM electrodes, which supports a diffusion-controlled mechanism.[32] A time square root increase was observed up to 150 h, when a leveling off occurred (Figure 5a). After annealing, a resistance increase of 9 Ω representing about 60% of R_T was measured (Figure 5b). For the sample annealed at 1673 K, the degradation was higher as expected with the increase in annealing temperature. The variations recorded as a function of annealing time are slightly different. By plotting the initial values of R_T determined at the beginning of each isothermal plateau as a function of the annealing temperature, a decrease in the initial value was determined up to 1573 K (Figure 6). Note that the initial values were taken at different temperatures. An increase in this value of R_T was observed at 1673 K. This increase is due to the fast reaction between LSM and YSZ at 1673 K that changed the interface even before any IS measurement. The R_T initial value extrapolated from Figure 6 is 4 times as low as the measured one. This extrapolated value, 4.0 Ω, was used to calculate ΔR_T at 1673 K, the highest

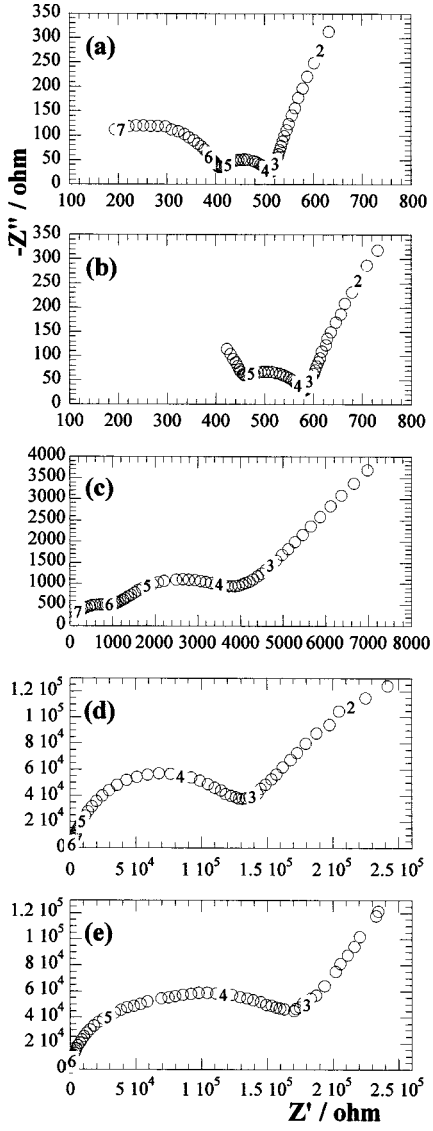

Figure 4. Complex impedance diagrams of the $La_{0.65}Sr_{0.35}MnO_3/Zr_{0.84}Y_{0.16}O_{1.92}$ electrode measured at 673 K in air: as-fired (a) and annealed for 200 h at 1373 K (b), 1473 K (c), 1573 K (d), and 1673 K (e).

annealing temperature. ΔR_T increased linearly with $t^{1/2}$ for annealing times up to 40 h (Figure 5a). For longer times, a decrease in the additional interface resistance was recorded. This is rather surprising, if one compares it to lower temperature behavior. At 1673 K, grain growth in YSZ occurred (Figure 7). Accordingly, a decreasing grain boundary density might be anticipated, resulting in a lower related blocking effect. It is also known that the introduction of manganese within the zirconia matrix during annealing may affect the sintering behavior of the electrolyte,[39] but at this stage, the origin of the decrease in the aging effect is still unknown. Nevertheless, for a 200 h period, the degradation of the electrical properties of YSZ at 1673 K remained higher than those previously recorded, which is in agreement with the behavior expected as a function of temperature (Figure 5b). Within this time interval,

(39) Linderoth, S.; Kuzjukevocz, A. In *Proceedings of the Fifth International Symposium on Solid Oxide Fuel Cells*; Stimming, U., Singhal, S. C., Tagawa, H., Lehnert, W., Eds.; The Electrochemical Society: Pennington, NJ, 1997; Vol. 40, p 1076.

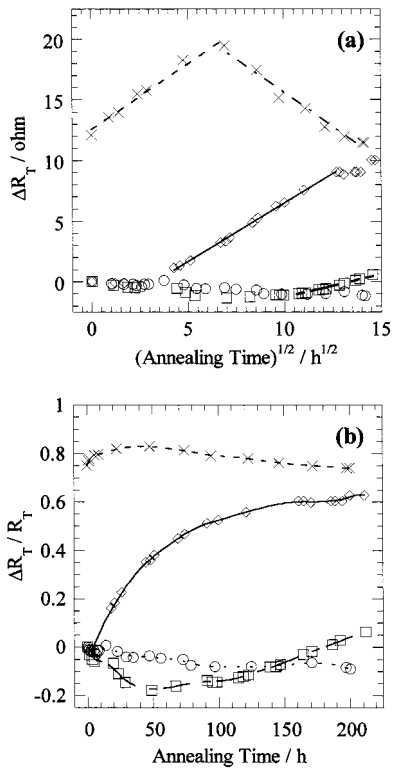

Figure 5. (a) Additional interface resistance and (b) relative increase in the additional interface resistance with annealing time. The annealing temperatures were (○) 1373, (□) 1473, (◇) 1573, and (×) 1673 K.

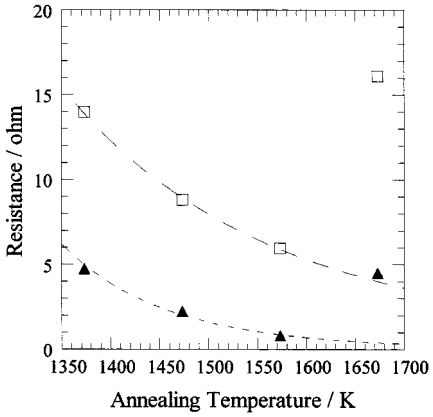

Figure 6. Initial values of (□) R_T and (▲) R_η as a function of the annealing temperature.

the higher the annealing temperature, the higher the aging rate. At 1673 K, the additional resistance represented nearly 80% of R_T.

When the sample was cooled to a measurement temperature of 673 K, the increase in the interface resistance observed at high temperature remained (Figure 4). The interface resistance is an increasing function of the annealing temperature. After annealing at 1573 K, R_T measured at 673 K is 260 times higher than before annealing. The adverse effect of high-temperature annealing on R_T comes mainly from the increasing amplitude of the medium-frequency arc, whose magnitude rises with the annealing temperature. Since YSZ grain boundary resistance is supposed to decrease after high annealing temperatures due to the YSZ grain growth (Figure 7), the increase observed in R_T can be attributed to additional microstructure block-

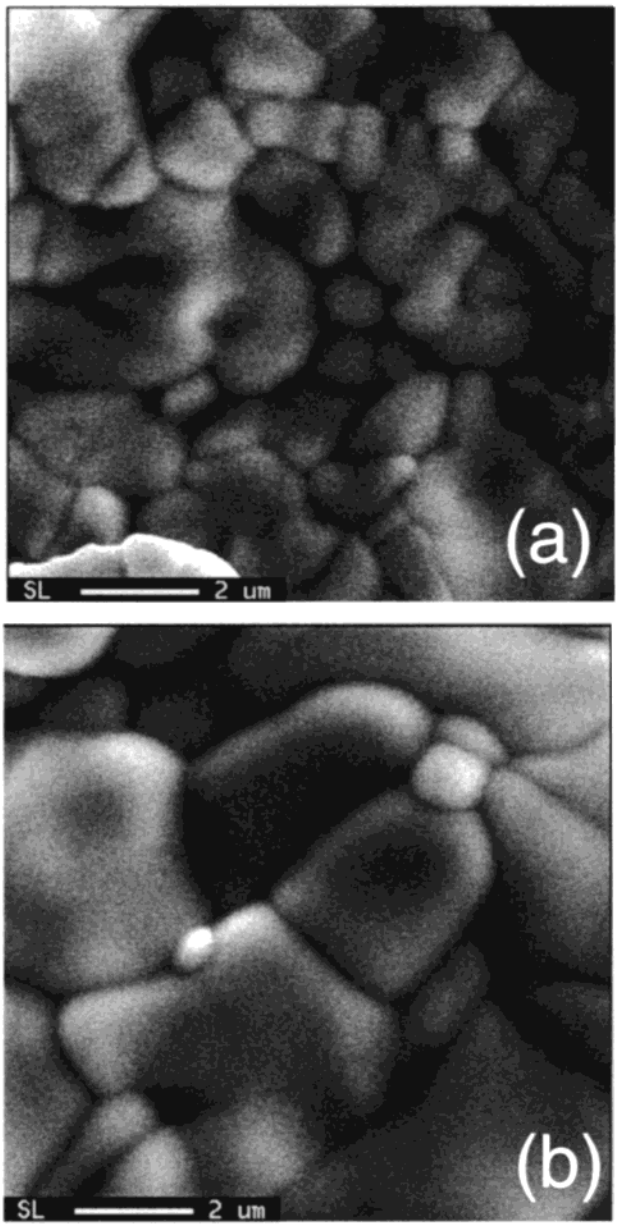

Figure 7. Scanning electron micrographs of the YSZ surface after annealing at 1673 K for (a) 34 h and (b) 200 h.

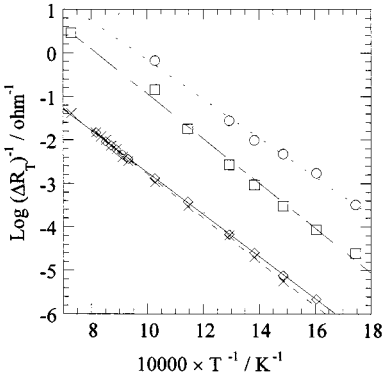

Figure 8. Arrhenius plots of $1/R_T$ after annealing at (○) 1373, (□) 1473, (◇) 1573, and (×) 1673 K.

ers. Figure 8 shows the Arrhenius diagram of the inverse of ΔR_T plotted after high-temperature annealing. At a given temperature, ΔR_T was calculated by the mathematical difference between the R_T values obtained

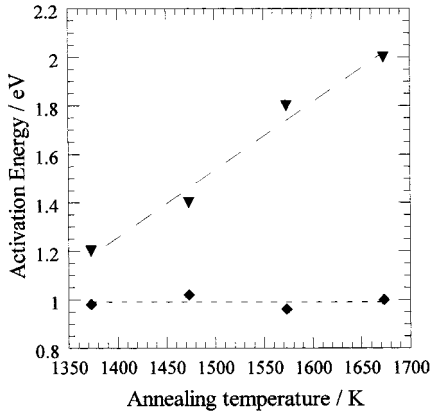

Figure 9. Activation energy of the additional (◆) interface and (▼) overpotential resistances after annealing for 200 h as a function of annealing temperature.

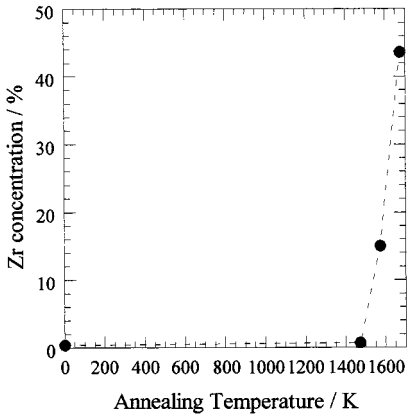

Figure 10. Zirconium concentration before and after 200 h of annealing as a function of annealing temperature.

after and before the annealing treatments. Regardless of the annealing temperature, the activation energy for electrical conduction was found to be close to 0.9 eV (Figure 9), as generally determined for conventional YSZ polycrystalline ceramics. The variation of R_T in the Arrhenius plot was meaningful since no time evolution of R_T was observed for different temperatures during cooling. It is worth emphasizing that the activation energy values (Figure 9) calculated from Figure 8 are related to the oxygen ion conduction and do not represent the activation energies for formation of the interfacial zirconate phases. This result means that the ionic conduction mechanism was not changed by the presence of this new resistive contribution. This represents the electric behavior expected from the additional microstructure blockers, which can be interpreted in terms of a simple decrease in the intimate contact area between YSZ and LSM. Thus, ΔR_T could be related to a microstructural change of the LSM/YSZ interface. The values of the additional interface resistance for samples annealed at 1673 K (Figure 5b) are only slightly higher than those obtained after annealing at 1573 K (Figure 8). EDS analysis confirmed qualitatively the accumulation of zirconates at the electrode top surface for samples annealed over 1473 K (Figure 10). This region was chosen because it has already been reported[17] that zirconate grows from the interface to the LSM layer. Each point of Figure 10 represents the arithmetic mean of the Zr content of 20 different points on the top of each LSM layer. All these results suggest that the adverse

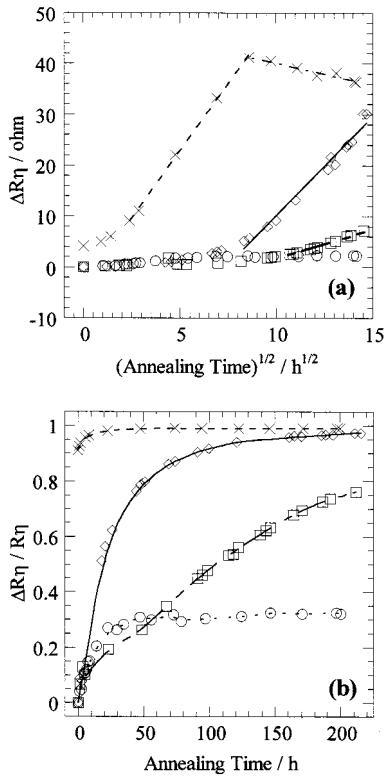

Figure 11. (a) Additional overpotential resistance and (b) the relative increase of the additional overpotential resistance with annealing time. The annealing temperatures were (○) 1373, (□) 1473, (◇) 1573, and (×) 1673 K.

effect on the interface resistance can be related to the formation and growth of lanthanum ($La_2Zr_2O_7$) and strontium ($SrZrO_3$) zirconates.

As for the interface resistance, the magnitude of the changes of the overpotential resistance R_η was described by using the additional overpotential resistance ΔR_η determined as the mathematical difference between the overpotential resistance measured at annealing time t and at $t = 0$. A positive ΔR_η value could thus be related to a degradation of the electrochemical performances of the electrodes investigated. The relative increase in the additional overpotential resistance was defined as the ratio $\Delta R_\eta/R_\eta$ measured at time t during the course of high-temperature annealing.

In agreement with similar measurements performed on pin-shaped LSM cathodes,[32] the electrochemical properties changed more intensely than the electrical ones (Figure 11). Even during annealing at 1373 K, the overpotential resistance increased whereas the interface resistance was nearly constant (Figure 5). At this temperature, a ΔR_η leveling off was observed over 40 h (Figure 11). However, no significant square root dependence of the annealing time was determined. On the other hand, at higher temperatures, the additional overpotential resistance was found to vary linearly with the square root of the annealing time, but not within the whole annealing period (Figure 11a). The square root law suggests that the changes observed are due to a diffusion-controlled mechanism, as already observed for the interface resistance. At 1573 K, a rapid increase in R_η was observed (Figure 11a). For annealing at 1673 K, the additional overpotential resistance corresponded to nearly 100% of the overpotential resistance after only 20 h (Figure 11b). It further suggests that the degradation of the electrochemical properties occurred before the thermal equilibrium was reached at this temperature (Figure 6). It is important to stress that such a large degradation required approximately 150 h at 1573 K (Figure 11b).

Figure 9 shows the activation energies for the electrical (◆) and electrochemical (▼) conduction determined from the Arrhenius diagrams of $1/R_T$ (Figure 8) and of the additional overpotential conductance ($1/\Delta R_\eta$). At a given temperature, ΔR_η was calculated by the mathematical difference between the R_η values obtained after and before the annealing treatments. The activation energy for the electrode processes increased after high-temperature annealing, whereas that of electrical conduction remained nearly constant (Figure 9). After annealing at 1373 K, the activation energy was found to be 1.2 eV, and for an aging temperature of 1673 K, this value increased to 2.0 eV. The higher the annealing temperature, the higher the activation energy. After isothermal treatment, a coalescence of LSM particles was observed, which resulted in both pore closing and fewer active reaction sites (Figure 12). A related degradation of the electrochemical properties could be anticipated,[40,41] and a shift of the frequency distribution of the electrode characteristics could be detected.[42,43] However, this microstructural evolution of the electrode should only represent a few tenths of a percent of the recorded changes. The increasing overpotential resistance may be caused by an additional change of the LSM/YSZ interface.[44] Accordingly, the recorded degradation of the overpotential resistance cannot be solely related to a simple reduction of the electrode contact area. It is likely to be due to a change in the electrode reaction mechanism itself because of the formation of insulating phases at the electrode/electrolyte interface.[26]

4. Conclusions

Impedance spectroscopy was shown to be a powerful on-line monitoring technique for the aging behavior of both the electrolyte resistance and the electrochemical properties of LSM-based cathodes. A peculiar feature of this technique is that the resulting in situ characterization can be performed without destroying the cell. Additional resistive contributions were observed for interface and overpotential resistances for temperatures over 1373 K. The recorded electrical degradations were associated with the formation of insulating phases already described to occur for similar systems in the same temperature range. However, a new insight gained was that the presence of these insulating phases seems

(40) Iorai, T.; Hara, T.; Uchimoto, Y.; Ogumi, Z.; Takehara, Z.-I. *J. Electrochem. Soc.* **1998**, *145*, 1999.
(41) Van Heuweln, F. H.; Bouwmeester, H. J. M. *J. Electrochem. Soc.* **1997**, *144*, 134.
(42) Kato, T.; Momma, A.; Kaga, Y.; Nagata, S.; Kasuga, Y. In *Proceedings of the Fifth International Symposium on Solid Oxide Fuel Cells*; Stimming, U., Singhal, S. C., Tagawa, H., Lehnert, W., Eds.; The Electrochemical Society: Pennington, NJ, 1997; Vol. 40, p 1150.
(43) Holtappels, P.; Jorgensen, M. J.; Primdhal, S.; Mogensen, M.; Bagger, C. In *Proceedings of the Third European Solid Oxide Fuel Cells Forum*; Stevens, P., Ed.; European Fuel Cell Forum: Oberrohrdorf, 1998; p 311.
(44) Umemura, F.; Amano, K.; Michibita, H.; Kimura, A. In *Proceedings of the Fourth International Symposium on Solid Oxide Fuel Cells*; Dokiya, M., Yamamoto, O., Tagawa, H., Singhal, S. C., Eds.; The Electrochemical Society: Pennington, NJ, 1995; Vol. 1, p 649.

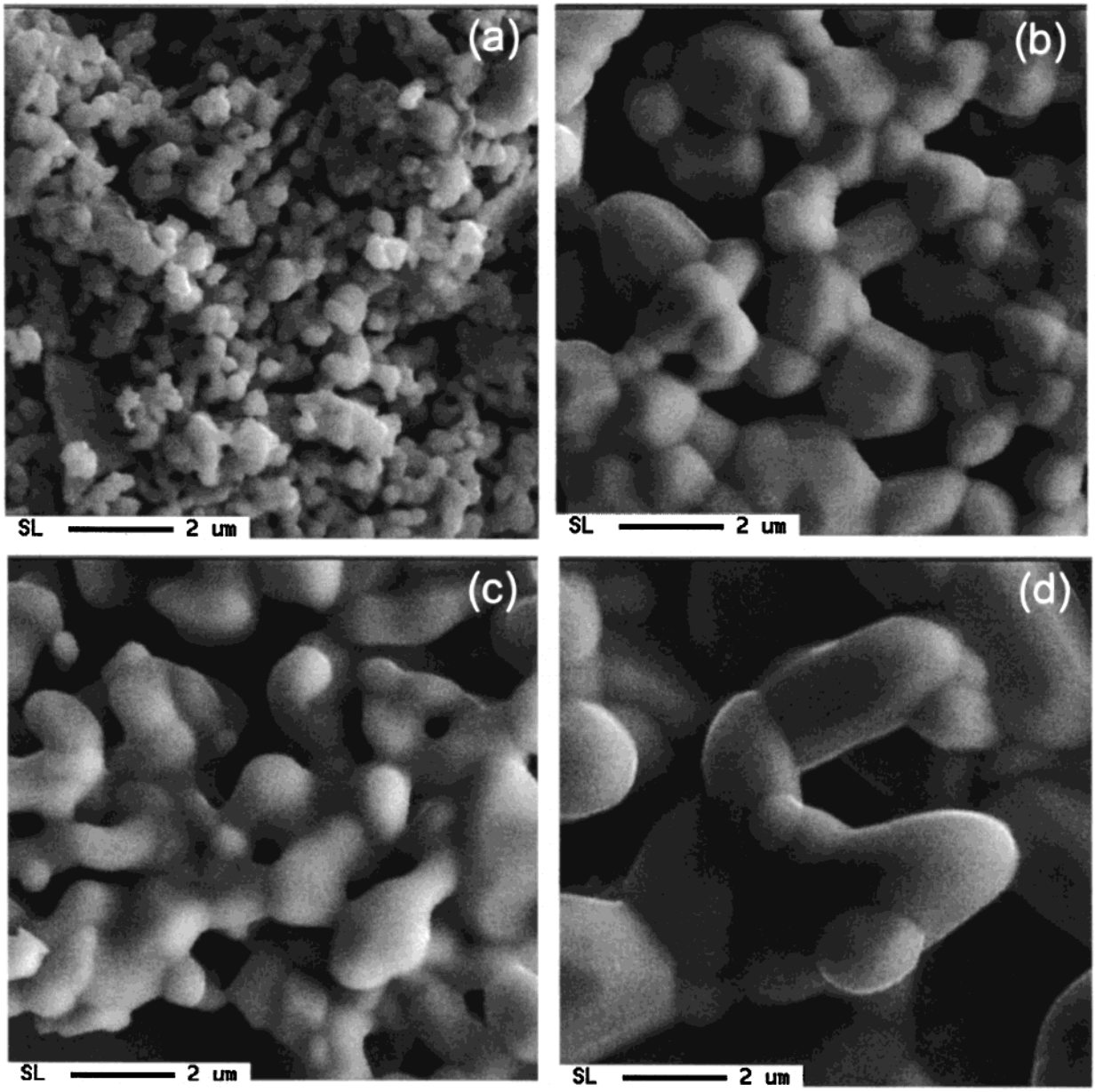

Figure 12. Scanning electron micrographs of the cathode material surface: as-fired (a) and after annealing at 1473 K (200 h) (b), 1673 K (34 h) (c), and 1673 K (200 h) (d).

to affect the electrical and overpotential resistances differently. The changes in the interface electrical properties can be interpreted in terms of a simple decrease in the intimate contact area between YSZ and LSM, which results in fewer contact points and an increase of interface resistance. No change in the conduction mechanism was detected as the activation energy for electrical conduction values was constant and close to that generally determined for YSZ. The formation of the insulating phases resulted in a strong reduction of the electrode reaction rate, which cannot be solely related to a simple reduction of the electrode contact area. It is likely to be due to a change in the electrode conduction mechanism, whose activation energies increased about 70% for samples annealed from 1373 to 1673 K.

Acknowledgment. This work was partially supported by CAPES and CNPq.

CM000656R